FLYWHEEL: JURNAL TEKNIK MESIN UNTIRTA

Homepagejurnal: http://jurnal.untirta.ac.id/index.php/jwl

Electrochemical Behavior, Structure, and Morphology of Electrodeposited Nickel on Copper Alloy Prepared from Sulphate Bath without Additive Addition

Bambang Soegijono[1,*], Ferry Budhi Susetyo[1,2], Hamdan Akbar Notonegoro[3], and Musfirah Cahya Fajrah[4]

[1] *Dept. of Physic, Universitas Indonesia, Depok 16424, Indonesia*
[2] *Dept. of Mechanical Engineering, Universitas Negeri Jakarta, Jakarta 13220, Indonesia*
[3] *Dept of Mechanical Engineering, Universitas Sultan Ageng Tirtayasa, Cilegon 42435, Indonesia*
[4] *Dept. of Physic, Institut Sains dan Teknologi Nasional, Jakarta 12640, Indonesia*

*Corresponding author: naufal@ui.ac.id

ARTICLE INFO

Received 31/03/2020
revision 22/04/2020
accepted 29/04/2020
Available online 30/04/2020

ABSTRACT

Nickel and nickel alloy has good chemical and physical properties to enhance corrosion resistance. Electrodeposited nickel layer are expected to improve the corrosion resistance of copper as substrates. The difference distance crystal plane of Nickel and Copper is about 0.02 – 0.03 Angstrom. The electrochemical behavior, structure, and morphology of electrodeposited nickel on a copper substrate in a sulfate solution were investigated. Electrodepositions of nickel layer were conducted at room temperature with various current densities (10 mA/cm^2, 20 mA/cm^2, and 30 mA/cm^2). Electrochemical behavior, structure, and morphology of the samples were analyzed by using a potentiostat, x-ray diffraction (XRD), and Scanning electron microscope (SEM). The x-ray diffraction patterns show that the nickel has a cubic FCC crystal system and space group Fm-3m. The current density during the electrodeposition process had influenced the crystallite parameter, crystallite size, and micro strain of nickel film deposited. Electrodeposited nickel with current density 30 m A/cm^2 shows the best corrosion resistance.

Keywords: *nickel; copper alloy; electrodeposition; sulphate solution*

1. INTRODUCTION

Electrodeposition is a simple process and low-cost approach which was utilized extensively to fabricate various metallic layers for different purposes [1–4]. Nickel and nickel alloy has good chemical and physical properties materials to enhance corrosion resistance [5–7]. The nickel layer's electrodeposition has been widely used in many industrial fields to improve decorative, protection, and wear properties [8–10]. Electrodeposition of nickel commonly are conducted on sulfate [11], sulfamate [12], chloride [13], and citrate [14] electrolyte solution.

Corrosion to metals occurs during an electrochemical oxidation reaction. Nickel layer shows excellent corrosion resistance in aggressive aqueous environments [9]. The stable passive film on the surface of nickel gave advantages to excellent corrosion resistance [15]. Moreover, the nickel layer shows better corrosion resistance with decrease crystallite size. Nasirpoury et al. had reported electrodeposition of nickel from watts bath solution using direct current (DC), pulsed current (PC), and pulsed reversed current (PRC) technique resulting in the crystallite size 41 nm, 30 nm, 36 nm respectively. It also found that the sample with the smallest crystallite size has the best corrosion resistance [16]. On the other hand, besides the size of crystallite and passive films, the nickel layer's corrosion resistance is strongly influenced by the microstructure

[17,18]. The microstructures of electrodeposited nickel is closely related to electrodeposition parameter such as current density [19–21], pH [22], and additive [19,23,24]. Zhao et al. were conducted electrodeposition of nickel with various current densities resulting in various grain (crystallite) size [8].

Therefore, this present work aims to prepare the electrodeposition nickel on Copper alloy using a sulfate solution without additive addition at different current densities. Nickels deposit to copper were one of the crystal plane distance difference was about 0.02-0.03 Angstrom. Electrodeposited nickels were analyzed by Potentiostat in 3.5% NaCl solution, Scanning electron microscope, and X-ray diffraction to determine crystal parameter. The results will show the necessity of Ni plating on Copper Alloy in a severe environment.

2. EXPERIMENTAL

2.1. Material Preparation

The electrodeposition of nickel was prepared from a sulfate bath at 250 ml fresh electrolyte solution. The electrolyte solutions were consisting of Nickel (II) sulfate hexahydrate ($NiSO_4.6H_2O$) with composition 0.25 M analytical grade chemical from Merck. The electrodepositions of nickel were conducted using D.C Power Supply for 2-hour durations to various samples. The cathode was a copper alloy with composition in Table 1, and the anode was a nickel plate (99.99%). The cathode was cut 1 cm x 1 cm x 0.3 cm and embedded on epoxy resin with 1 cm x 1 cm area of the surface is left open. Before the electrodeposition process, the cathode's surface was prepared using 1000 mesh up to 3000 mesh abrasive papers. It was followed by cleaning cathodes with acetone in the ultrasonic cleaner for 10 minutes. Distance between the anode (nickel) and the cathode (copper alloy) was maintained about 5 cm during the electrodeposition process. The electrodepositions of nickel were conducted with various current densities of 10 mA/cm^2, 20 mA/cm^2, and 30 mA/cm^2. The sample obtained at current density ten mA/cm^2, 20 mA/cm^2, and 30 mA/cm^2 was designated as Ni-10, Ni-20, and Ni-30, respectively.

Table 1. The chemical compositions of copper substrates.

Element	Al (wt.%)	Ni (wt.%)	Cu (wt.%)
Concentration	2.977	2.9016	balance

2.2. Electrochemical Investigation

The electrochemical investigation was used cell of the three-electrode (Digi-Ivy DY2311) equipment made from Austin Texas USA, where silver/silver chloride (Ag/AgCl) as a reference electrode (RE) and platinum wire (Pt) as a counter electrode (CE). The electrochemical investigation was conducted with scan rates of 50 mV/s. and scans from -1.5 V to 0.5 V, with sensitivity 0.003 (A/V) in 100 mL 3.5% NaCl fresh solution. The corrosion current density (I_{corr}) and corrosion potential (E_{corr}) can be determined by extrapolating the linear portions of the potentiostat polarization plots to the intersection. Meanwhile, the corrosion rate can be calculated using corrosion current density with the equation [25] :

$$CorrosionRate(mmpy) = C\frac{MI_{corr}}{n\rho} \quad (1)$$

Where, ρ=density of nickel (8.098 g/cm^3), I_{corr}=corrosion current density (A/cm^2), M=atomic weight of nickel (58.69 g/mol), n=number of electrons involved (2), and C=constant (3.27). Moreover, the electrochemical investigation was used open circuit potential measurements were carried out from 0 to 1200 seconds, with sampling retrieval time per 2 seconds.

2.3. Structure

The crystalline structure of the electrodeposited nickel was identified by x-ray diffraction (PANalytical X-ray Diffractometer (XRD) with CuKa_ radiation) and scans from 20° to 90° with the resolution of 0.002°. Highscore plus software was used to refine the XRD pattern to obtained crystal parameters. The results of the X-ray diffraction pattern refinement achieved with Rwp and GOF below 10 % and two, respectively.

2.4. Surface Morphology

A scanning electron microscope (SEM) FE-SEMFEI INSPECT F50 Analyzer was used to observe the surface morphology of samples. The observations of the sample conducted 25000 x magnifications were scanning electron microscope connected to monitor of the PC apparatus.

3. RESULTS AND DISCUSSION

3.1 Electrochemical Test

3.1.1. Potentiodynamic Polarization

The common test used to determine the corrosion behavior of metals is potentiodynamic polarization. In order to explore corrosion resistance, potentiodynamic polarization measurements were employed to examine samples in a simulated seawater solution containing 3.5 wt. % NaCl [26–28]. Figure 1 shows the potentiodynamic polarization plot curve for the various samples in a 3.5% NaCl aqueous solution at room temperature and a describe typical active-passive-trans passive corrosion behavior. These results seem similar to other research conducted with the potentiodynamic measurements of nickel [15,29]. Their corresponding corrosion potential (E_{corr}), corrosion current density (I_{corr}), and corrosion rate were summarized in table 2, where the corrosion rate was calculated used corrosion current with equation (1).

The cathodic reaction at the potentiodynamic polarization curve corresponded to the evolution of the hydrogen, and the anodic polarization curve was related to the corrosion resistance [30]. An active anodic process for an electrodeposited nickel was observed when applied potential shifted onto the anodic region. For the Ni-30 sample, a corrosion potential (E_{corr}) about -0.841 V with current corrosion (I_{corr}) 1.64 x 10^{-5} A was

recorded. The Ni-30 sample has better corrosion resistance than Ni-10 and Ni-20 sample (see table 2).

Table 2. Corrosion current density, corrosion potential, corrosion rate and OCP potential electrodeposited nickel at various current densities

No	Sample	I_{Corr} (A/cm^2)	E_{Corr}(V)	Cor Rate (mmpy)	E_{OCP}(V)
1	Ni-10	2.64×10^{-5}	-0.787	0.285	-0.250
2	Ni-20	3.64×10^{-5}	-0.892	0.392	-0.224
3	Ni-30	1.64×10^{-5}	-0.841	0.177	-0.270

Corrosion potential (E_{corr}) of the Ni-30 sample was shifted positively about 51 mV compared with the Ni-20 sample. This indicated the Ni-20 sample more anodic than the Ni-30 sample [31]. Moreover, the corrosion potential of the Ni-10 sample is more anodic than a various sample of electrodeposited nickel.

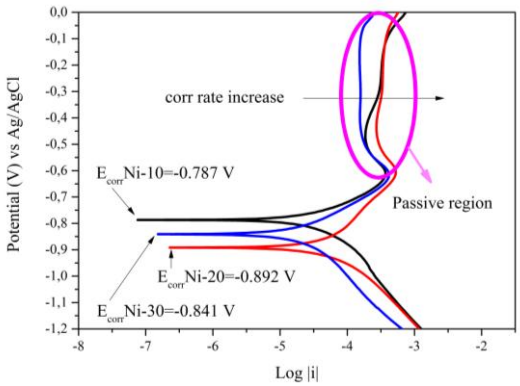

(a)

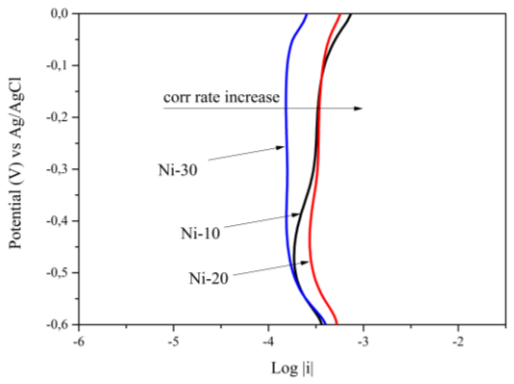

(b)

Figure 1. Potentiodynamic Polarization curve of electrodeposited nickel sample in 3.5% NaCl aqueous solution: (**a**) Corrosion potential; (**b**) Comparative passive region.

The passive region is presented in figure 1 (a), and the comparative passive region is presented in figure 1 (b) resulting from potentiodynamic polarizations in 3.5% NaCl aqueous solution. This passive region is one kind of factor that would be affecting corrosion resistance behavior [32]. The nickel layer was in the active state from corrosion potential (E_{corr}) to about -0.6 V, and then in the passive state at potentials higher than -0.6 V irrespective of the nickel layer from varies current densities of electrodeposition. As we can see in figure 1, (b) sample Ni-20 has shifted to negative log current, followed Ni -10 and Ni-30 samples. Compared to figure 1 (b) with table 2, we can see the sample which shifted to negative log current has less corrosion rate. This is related to Park et al. work were investigating passive films on the nickel [15].

3.1.2. Cyclic Voltammetry

For the investigation of anodic and cathodic behavior of the nickel layer, cyclic voltammetry was recorded with a scan rate of 50 mV/s of various samples in 100 mL 3.5% NaCl aqueous solution. Typical cyclic voltammetry for various samples in room temperature solution is presented in figure 2.

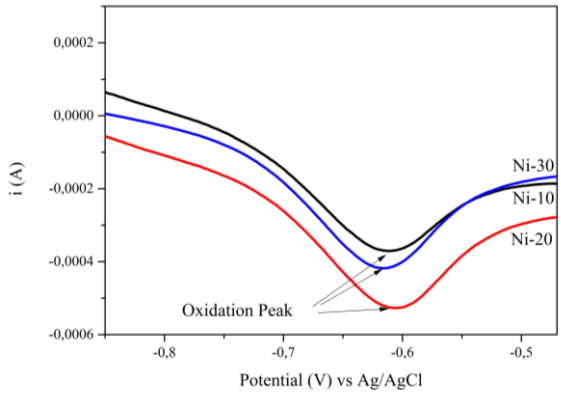

(a)

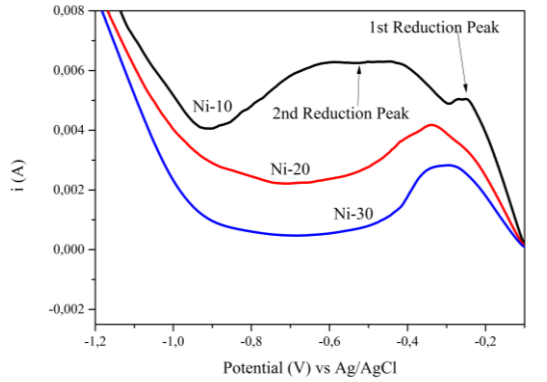

(b)

Figure 2. Cyclic Voltammetry curve of electrodeposited nickel sample were conducted in 3.5% NaCl aqueous solution: (a) Oxidation region; (b) Reduction region

The potential scan was initiated at -1.5 V to 0.5 V for an anodic sweep and reversed for a cathodic sweep. On the anodic sweep, oxidation commenced at about -0.75 V, followed by active anodic dissolution up to -0.45 V for an electrodeposited nickel. Once the passive NiO film is formed, the anodic dissolution becomes steady at about -0.15 mA for Ni-30 sample, -0.2 mA for Ni-10 sample, and -0.3 mA for Ni-20 sample (figure 2 (a)). As we can see in figure 2 (b) after reversing scan 0.5 V to -1.5 V, the reduction peak of the three samples has different behavior. Sample Ni-10 has the biggest reduction peak

than Ni-20 and Ni-30 samples, but sample Ni-10 has two reduction peaks. This probably means two process reductions as we can see on the following equation [33]:

$$NiO + H_2O = Ni(OH)_2 \quad (2)$$

$$NiO + 2H^+ + 2e = Ni(OH)_2 \quad (3)$$

For the cathodic sweep sample Ni-10, reduction commenced at about -0.1 V, followed by a cathodic reduction up to -0.9-V. Moreover, for the cathodic sweep sample Ni-20 and Ni-30, reduction commenced at about -0.1 V, followed by a cathodic reduction up to -0.5 V.

3.1.3. Open Circuit Potential

Figure 3 presents the open circuit potential of electrodeposited nickel with different current density starting from 0 to 1200 second in 3.5% NaCl aqueous solution. The steady-state potential for Ni-10 sample (-0.250 V) was attained within 300 seconds, and for Ni-20 and Ni-30 samples, it takes more than 1200 seconds to reach a steady state.

Generally, the electrodeposited nickel sample shows the continuous shift of the potential open circuit to positive values, indicating additional passivation over the period of measurement (1200 seconds).

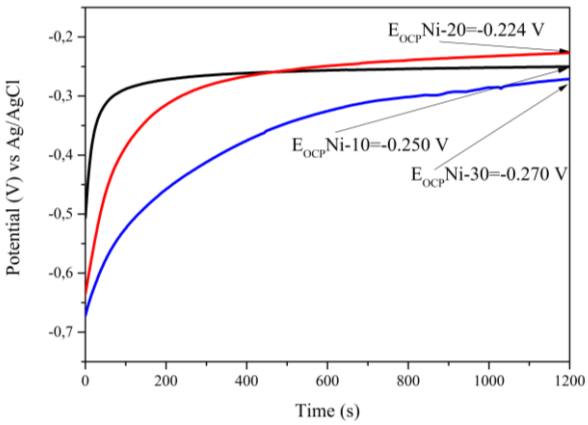

Figure 3. Open circuit potential curves of electrodeposited nickel samples were conducted in 3.5%-NaCl.

Based on the electrochemical investigations, Ni-30 has better corrosion resistance, the highest negative OCP voltage, lowest peak reduction, and shift to the left side of the passive region. The lowest corrosion resistance is on the Ni-20 with the lowest negative OCP voltage, middle reduction peak, and shift to the right side of the passive region.

3.2. X-Ray Diffraction

The XRD patterns of electrodeposited Nickel show in figure 4, peaks diffractions of the three samples show patterns of diffraction peaks of (111), (002), and (022). The crystal system of samples is Cubic FCC with Space Group Fm-3m obtained from Rietveld refinement analysis using Highscore plus software with ICSD 98-004-3379 (ref. Code). Various previous research reported a similar pattern and crystal system with our research [11,13,17,19,34].

The average crystallite sizes obtained from highscore plus software are summarized in Table 3. It shows various crystallite sizes of the electrodeposited nickel, and they are not linearly with current density. These results are contradictive with Zhao et al. report of electrodeposition of nickel in sulfamate solution.

The crystallite size increases with the increase of the current density [8]. The Ni-30 sample has the smallest crystallite size, and the Ni-20 sample has a larger crystallite size. It should be noted that the smaller crystallite size would increase the corrosion resistance of the nickel [11,16]. The correlation between crystallite size and corrosion rates are presented in figure 5. It shows the crystallite size closely linearly related to corrosion resistance for the samples, and these are also related to previous reports [35,36]. Furthermore, shifting the crystallite size to a smaller value, lead to higher microstrain and the density value of the electrodeposited nickel ($\rho = 9{,}03\ g/cm^3$).

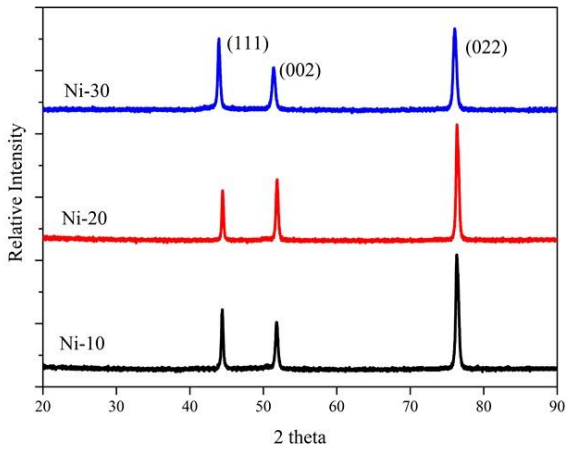

Figure 4. The XRD pattern of various current densities electrodeposited nickel.

Table 3. Crystal parameter of various current densities electrodeposited nickel.

Parameter	Sample		
	Ni-10	***Ni-20***	***Ni-30***
Crystal System	Cubic FCC	Cubic FCC	Cubic FCC
Space Group	Fm-3m	Fm-3m	Fm-3m
a=b =c(Å)	3.5182	3.5208	3.5077
V (Å3)	43.568	43.642	43.157
Density, ρ (g/cm³)	8.95	8.93	9.03
Crystallite size (nm)	38.78	49.82	23.82
Micro strain (%)	0.131	0.081	0.165
Rwp (%)	8.08	9.83	7.77
GOF	1.38	1.85	1.19

The crystallite sizes of the nickel layer were probably influenced by (002) crystal plane peak intensity. The increase of (002) peak intensity would affect the crystallite size. This was also reported by other

researchers [8]. The (002) peak intensity of Ni-10, Ni-20, and Ni-30 samples are 2041, 2389, and 1873 respectively. The peak intensity of (111) for FCC metal also gives a contribution to the corrosion resistance. If the (111) peak is higher, it will be increased corrosion resistance [37].

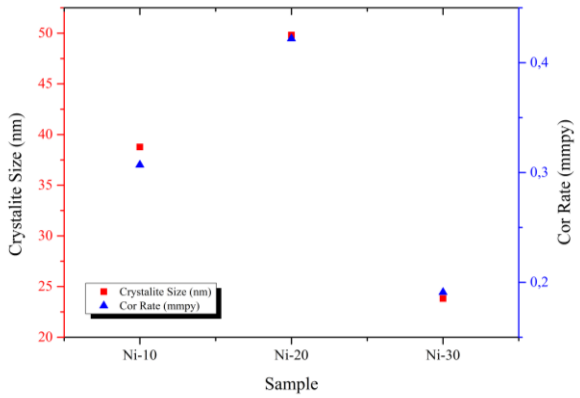

Figure 5. The correlation between crystallite size and the corrosion rate of electrodeposited nickel.

As we can see in table 4, the peak intensity (111) of sample Ni-10, Ni-20, and Ni-30 are 2441, 2069, and 2789 respectively. The sample of Ni-30 shows the highest peak than the Ni-10 and Ni-20 samples. This means that the sample Ni-30 would have less corrosion rate than Ni-10 and Ni-20 samples. By comparing the peak intensity of (111) in table 4, It is clearly seen that the corrosion rate is closed linearly with the (111) peak intensity. Shifting to higher current density would affect the decreasing intensity of (022) peak.

Table 4. Peak intensity electrodeposited nickel sample at various current densities.

No	Sample	Intensity (111)	Intensity (002)	Intensity (022)
1	Ni-10	2441	2041	4176
2	Ni-20	2069	2389	4095
3	Ni-30	2789	1873	3066

Table 5 is the FWHM of electrodeposited nickel sample at various current density. As we can see the Ni-30 sample have higher FWHM than others. The smallest FWHM are seen on Ni-20 sample.

Table 5. FWHM electrodeposited nickel sample at various current densities.

No	Sample	FWHM (111)	FWHM (002)	FWHM (022)
1	Ni-10	0.2437	0.2562	0.3320
2	Ni-20	0.2337	0.2450	0.3004
3	Ni-30	0.3269	0.3346	0.4133

3.3 Scanning Electron Microscope Observation

The surface morphology of the electrodeposited nickel with different current densities was studied by Scanning Electron Microscope. The depositions time were conducted for a fixed time about 120 min for electrodeposited nickel sample at room temperature.

Figure 6 shows the surface morphology of sample Ni-10, Ni-20, and Ni-30 were collected from Scanning Electron Microscope with magnification 25000 X. It seems that the Ni-20 has to show larger grain than other samples, as shown in figure 6 (b). The samples Ni-10 show clearly smooth and compact surface with fine granules, as we can see in figure 6 (a). The sample Ni-30 shows small grain that is distributed on large grain. This phenomenon probably correlated with the FWHM in table 5. The highest average FWHM is in the Ni-30 sample that shows a compact small grain around the big grain. The surface morphology of material would affect the corrosion rate of the sample [17]. Based on Table 2, the Ni-20 sample has resulting highest corrosion rate than the other electrodeposited nickel samples. This behavior was caused by surfaces of sample Ni-20 has a larger grain than the other electrodeposited nickel samples.

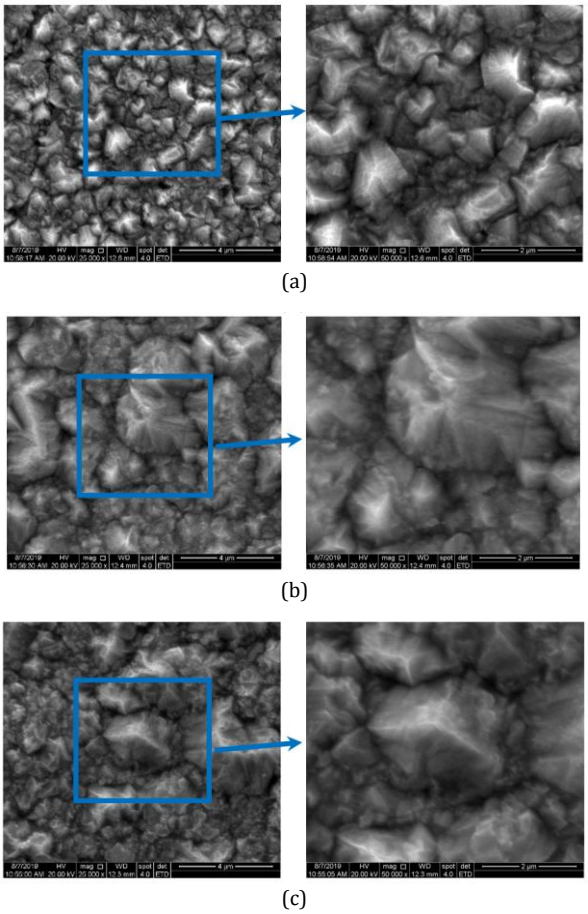

(a)

(b)

(c)

Figure 6. Scanning electron microscope images of samples were show comparison of various electrodeposited nickel at different current densities: a)Ni-10, b)Ni-20, c)Ni-30.

4. CONCLUSION

The X-ray diffraction patterns show that the nickel has crystal system Cubic FCC and space group Fm-3m. The current densities are affecting the reduction of crystal parameter and increase the density and lead to a

reduction in crystallite size. The increase of density is probably due to Crystal plane distances of nickel tend to be forced close to a crystal plane of Copper, which as a substrate during electrodeposition, where Copper crystal plane distance is smaller. The crystallite size and peak intensity of (111) has a correlation with the corrosion resistance. Smallest crystallite size and highest peak intensity of (111) are affecting the better corrosion resistance. Electrodeposited nickel with current density 30 mA/cm^2 shows the best corrosion resistance.

ACKNOWLEDGEMENT

The authors thanks for financial support from Ministry of Research, Technology and Higher Education of the Republic of Indonesia Kementrian Riset, Teknologi dan Pendidikan Tinggi, Hibah Penelitian Disertasi Doktor No : NKB-1827/UN2.R3.1/HKP.05.00/2019.

REFERENCES

1. Ming Z, Chunkai L, Gang Z, Yu S, Ding F, Jiankang H. Modeling and control of consumable DE-GMAW process. J Manuf Process. 2016;24:293–7.
2. Chai Z, Jiang C, Zhao Y, Wang C, Zhu K, Cai F. Microstructural characterization and corrosion behaviors of Ni-Cu-Co coatings electrodeposited in sulphate-citrate bath with additives. Surf Coatings Technol. 2016;307:817–24.
3. Thurber CR, Ahmad YH, Sanders SF, Al-Shenawa A, D'Souza N, Mohamed AMA, et al. Electrodeposition of 70-30 Cu-Ni nanocomposite coatings for enhanced mechanical and corrosion properties. Curr Appl Phys. 2016;16(3):387–96.
4. Abdulwahab M, Fayomi OSI, Popoola API. Structural evolution, thermomechanical recrystallization and electrochemical corrosion properties of Ni-Cu-Mg amorphous coating on mild steel fabricated by dual-anode electrolytic processing. Appl Surf Sci. 2016;375:162–8.
5. Wang J, Xu J, Zhang X, Ren X, Song X, Chen X. An investigation of surface corrosion behavior of Inconel 718 after robotic belt grinding. Materials (Basel). 2018;11(12):1–14.
6. Genna S, Trovalusci F, Ucciardello N, Tagliaferri V. Improving performance of an open cell aluminium foam through electro-deposition of nickel. Materials (Basel). 2019;12(1).
7. Riyanto, Rofida I. Preparation and application of nickel plating on copper electrode (NPCE) for uric acid analysis in human urine using cyclic voltammetry. Int J Electrochem Sci. 2019;14(3):2290–304.
8. Zhao H, Liu L, Zhu J, Tang Y, Hu W. Microstructure and corrosion behavior of electrodeposited nickel prepared from a sulphamate bath. Mater Lett. 2007;61(7):1605–8.
9. Jinlong L, Yang M, Suzuki K, Miura H, Zhang Y. Comparison of corrosion resistance of electrodeposited pure Ni and nanocrystalline Ni–Fe alloy in borate buffer solution. Mater Chem Phys. 2017;202:15–21.
10. Zhu Z, Zhu D, Qu N. Effects of simultaneous polishing on electrodeposited nanocrystalline nickel. Mater Sci Eng A. 2011;528(24):7461–4.
11. Cheng W, Ge W, Yang Q, Qu X. Study on the corrosion properties of nanocrystalline nickel electrodepositied by reverse pulse current. Appl Surf Sci. 2013;276:604–8.
12. López JR, Stremsdoerfer G, Trejo G, Ortega R, Pérez JJ, Meas Y. Corrosion Resistance of Nickel Coatings Obtained by Electrodeposition in a Sulfamate Bath in the Presence of Samarium (III). Int J Electrochem Sci. 2012;7:12244–53.
13. Winiarski J, Cie B, Kunicki P, Szczygie B. Applied Surface Science Corrosion of nanocrystalline nickel coatings electrodeposited from choline chloride : ethylene glycol deep eutectic solvent exposed in 0 . 05 M NaCl solution. Appl Surf Sci J. 2019;470(November 2018):331–9.
14. Chaoqun L, Xinhai L, Zhixing W, Huajun G. Mechanism of Nanocrystalline Nickel Electrodeposition from Novel Citrate Bath. Rare Met Mater Eng. 2015;44(7):1561–7.
15. Park K, Ahn S, Kwon H. Effects of solution temperature on the kinetic nature of passive film on Ni. Electrochim Acta. 2011;56(3):1662–9.
16. Nasirpouri F, Sanaeian MR, Samardak AS, Sukovatitsina E V., Ognev A V., Chebotkevich LA, et al. An investigation on the effect of surface morphology and crystalline texture on corrosion behavior, structural and magnetic properties of electrodeposited nanocrystalline nickel films. Appl Surf Sci. 2014;292:795–805.
17. Zamanzad-Ghavidel MR, Raeissi K, Saatchi A. The effect of surface morphology on pitting corrosion resistance of Ni nanocrystalline coatings. Mater Lett. 2009;63(21):1807–9.
18. Belhamel K, Kheraz H, Ludwig R, Nguen TKD, Allsop N, AL-Juaid SS. Electrodeposition and morphology analysis of nickel nanoparticles from sulphate bath. e-Journal Surf Sci Nanotechnol. 2010;8(May):227–32.
19. Wasekar NP, Haridoss P, Seshadri SK, Sundararajan G. Influence of mode of electrodeposition, current density and saccharin on the microstructure and hardness of electrodeposited nanocrystalline nickel coatings. Surf Coatings Technol. 2016;291:130–40.
20. Rashidi AM. A Galvanostatic Modeling for Preparation of Electrodeposited Nanocrystalline Coatings by Control of Current Density. J Mater Sci Technol. 2012;28(12):1071–6.
21. Liu M, Liu H, Wang D, Liu B, Shi Y, Li F, et al. Effect of nanodiamond concentration and the current density of the electrolyte on the texture and mechanical properties of Ni/Nanodiamond composite coatings produced by electrodeposition. Materials (Basel). 2019;12(7).
22. Seo MH, Kim DJ, Kim JS. The effects of pH and temperature on Ni-Fe-P alloy electrodeposition from a sulfamate bath and the material properties of the deposits. Thin Solid Films. 2005;489(1-2):122–9.
23. Zhu YL, Katayama Y, Miura T. Effects of coumarin and saccharin on electrodeposition of Ni from a hydrophobic ionic liquid. Electrochim Acta. 2014;123:303–8.
24. Zhu YL, Katayama Y, Miura T. Effects of acetone and thiourea on electrodeposition of Ni from a hydrophobic ionic liquid. Electrochim Acta. 2012;85:622–7.
25. Zaki Ahmad. • ISBN: 0750659246 • Pub. Date: September 2006 • Publisher: Elsevier Science & Technology Books. 2006.
26. Aydin G, Yazici A. Effect of quenching and tempering temperature on corrosion behavior of boron steels in 3.5 wt.% NaCl solution. Int J Electrochem Sci. 2019;14(3):2126–35.
27. Kang W, Gao Z, Liu Y, Wang L. Effect of flow rate on corrosion behavior and hydrogen evolution potential of X65 steel in 3.5% NaCl solution. Int J Electrochem Sci. 2019;14(3):2216–23.
28. Tang J, Hu Y, Wang H, Zhu Y, Wang Y, Nie Z, et al. Complicated synergistic effects between three corrosion inhibitors for Q235 steel in a CO 2 -saturated 3.5 wt% NaCl solution. Int J Electrochem Sci. 2019;14(3):2246–64.
29. Fattah-alhosseini A, Naseri M, Gashti SO, Vafaeian S, Keshavarz MK. Effect of anodic potential on the electrochemical response of passive layers formed on the surface of coarse- and fine-grained pure nickel in borate buffer solutions. Corros Sci. 2018;131(November 2017):81–93.
30. Gu C, Lian J, He J, Jiang Z, Jiang Q. High corrosion-resistance nanocrystalline Ni coating on AZ91D magnesium alloy. Surf

Coatings Technol. 2006;200(18-19):5413–8.

31. Gu CD, You YH, Yu YL, Qu SX, Tu JP. Microstructure, nanoindentation, and electrochemical properties of the nanocrystalline nickel film electrodeposited from choline chloride-ethylene glycol. Surf Coatings Technol. 2011;205(21-22):4928–33.

32. Trompette JL, Massot L, Vergnes H. Influence of the oxyanion nature of the electrolyte on the corrosion/passivation behaviour of nickel. Corros Sci. 2013;74:187–93.

33. Iida M, Ohtsuka T. Ellipsometry of passive oxide films on nickel in acidic sulfate solution. Corros Sci. 2007;49(3):1408–19.

34. Ni H, Li P, Wang Z, Zou Z, Zhao M, Wang L, et al. Fabrication and characterization of nanocrystalline nickel with a grain size gradient by direct current electrodeposition. Int J Electrochem Sci. 2019;14(9):8429–38.

35. Бэ QINL, Jian-she L, Qing J. Effect of grain size on corrosion behavior of electrodeposited bulk nanocrystalline Ni. Trans Nonferrous Met Soc China. 2009;20(1):82–9.

36. Yang Z, Liu X, Tian Y. Fabrication of super-hydrophobic nickel film on copper substrate with improved corrosion inhibition by electrodeposition process. Colloids Surfaces A Physicochem Eng Asp. 2019;560(October 2018):205–12.

37. Jinlong L, Tongxiang L, Chen W. Effect of electrodeposition temperature on grain orientation and corrosion resistance of nanocrystalline pure nickel. J Solid State Chem. 2016;240:109–14.